Supplementary file

Nitrogen- and chemical-assisted steam huff-and-puff of heavy oil in heterogeneous microfluidic pore network

Tao Wei[1], Jianmei Yu[1], Qiuying Cao[1], Wenjie Han[1], Jinping Liang[1], Rui Wu [2,*]

[1] *Exploration and Development Research Institute, Dongying 257100, P. R. China*

[2] *School of Mechanical Engineering, Shanghai Jiao Tong University, Shanghai 200240, P. R. China*

E-mail address: weitao819.slyt@sinopec.com (T. Wei); yujianmei228.slyt@sinopec.com (J. Yu); caoqiuying.slyt@sinopec.com (Q. Cao); hanwenjie.slyt@sinopec.com (W. Han); liangjinping.slyt@sinopec.com (J. Liang); ruiwu@sjtu.edu.cn (R. Wu).

[*]Corresponding author (ORCID: 0000-0002-9943-1710 (R. Wu))

Wei, T., Yu, J., Cao, Q., Han, W., Liang, J., Wu, R. Nitrogen- and chemical-assisted steam huff-and-puff of heavy oil in heterogeneous microfluidic pore network. Capillarity, 2026, 19(1): 1-14.

The link to this file is: https://doi.org/10.46690/capi.2026.04.01

Text S1: Test parameters of oil reservoir or ODA

Reservoir properties such as oil viscosity, core wettability, and particle size distribution significantly influence interfacial migration processes. In this study, these parameters were rigorously measured.

S1.1 Rheological property

The heavy oil sample was obtained from the Shengli Oilfield, and its rheological properties were characterized using a Brookfield DV2T digital rotational rheometer (Fig. S1). The oil exhibits temperature-dependent rheological behavior. Below 60 °C, it displays non-Newtonian shear-thinning characteristics, with viscosity being sensitive to shear rate. Above 60 °C, however, the oil behaves as a Newtonian fluid, with viscosity becoming independent of shear rate and primarily dependent on temperature.

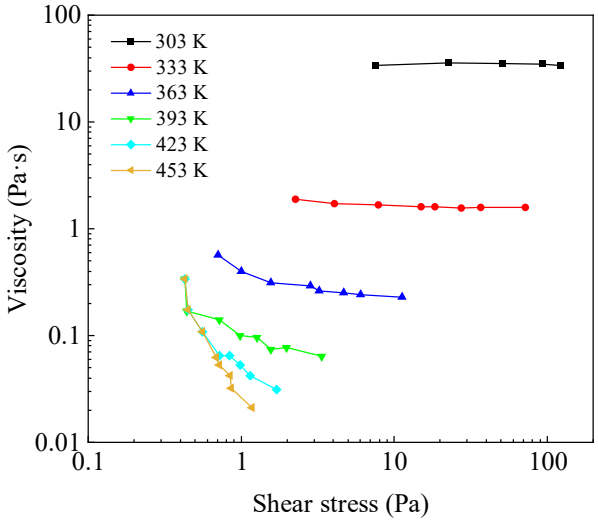

Fig. S1. Rheological properties of oil sample.

S1.2 Interfacial tension of the oil displacement agent

The oil displacement agent (ODA), procured from Shengli Oilfield Company, is a hydrophilic surfactant solution. The oil–water interfacial tension between heavy oil and ODA was measured using a spinning drop tensiometer (TX500C+). The measured interfacial tension evolution exhibited three characteristic stages: an initial stage, a dynamic stage, and a final equilibrium stage. The results confirmed that ODA reduces the interfacial tension to an ultralow level over a wide temperature range (Fig. S2), reaching 1.6 × 10^{-3} mN/m at 60 °C, 1.1 × 10^{-3} mN/m at 90 °C, and 9.5 × 10^{-4} mN/m at 120 °C.

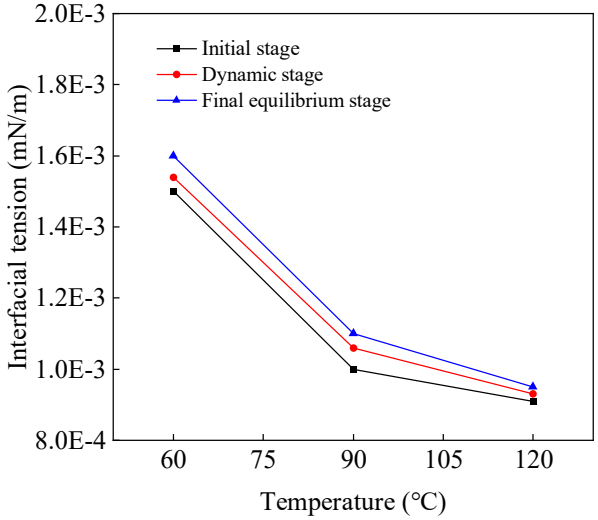

Fig. S2. Interfacial tension between heavy oil and ODA at different temperature.

S1.3 Particle size distribution

The particle size distribution of the oilfield core sample was determined using a Malvern Mastersizer 3000 laser particle size analyzer (Fig. S3). The particles range from 52 to 350 μm, revealing significant heterogeneity.

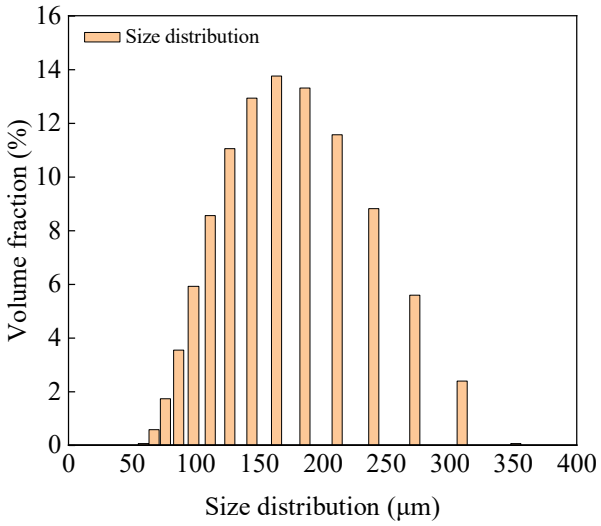

Fig. S3. Particle size distribution of core sample.

S1.4 Wettability

The wettability of the core samples was characterized by measuring the contact angle of heavy oil droplets on the core surface using a Krüss DSA25S goniometer via the sessile drop method in ambient air. As shown in Fig. S4, the measured contact angle is approximately 68.3°. The results demonstrate that the formation is predominantly oleophilic.

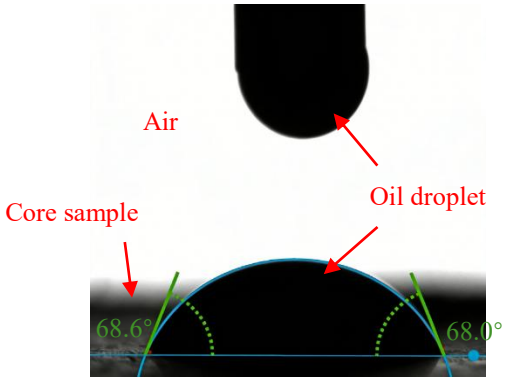

Fig. S4. The contact angle of heavy oil and core sample.

As shown in Fig. S5(a), the meniscus morphology at the pore throats is convex toward the oil phase, indicating that the water phase acts as the non-wetting fluid. Furthermore, as illustrated in Fig. S5(b), the heavy oil preferentially spreads along the channel walls and forms distinct corner films, demonstrating strong wettability towards the chip surface. Therefore, it can be concluded that the microfluidic chip exhibits strong oleophilicity (oil-wet characteristics).

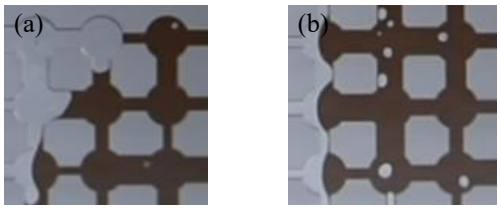

t = 260 s t = 485 s

Fig. S5. Phase distribution of heavy oil and water within the porous network during the injection process at (a) t = 260 s; (b) t = 485 s. Here, black regions represent the heavy oil phase, while gray regions represent the deionized water phase. The injection direction is from right to left.

Text S2: The unit zone based on the well configuration provided by Shengli Oilfield Company

The Shengli Oilfield adopts an inverted nine-spot well pattern to establish a more uniform and stable reservoir pressure field. In this pattern, the well spacing is 50 m, the steam-injection heating diameter is 100 m, and the average reservoir thickness is approximately 5 m. Under these conditions, the flow and pressure distributions between injection and production wells exhibit strong directional characteristics. Therefore, the diagonal injection–production well pair was selected as the representative analysis unit (Fig. S6), because it corresponds to the longest flow path and the maximum pressure gradient.

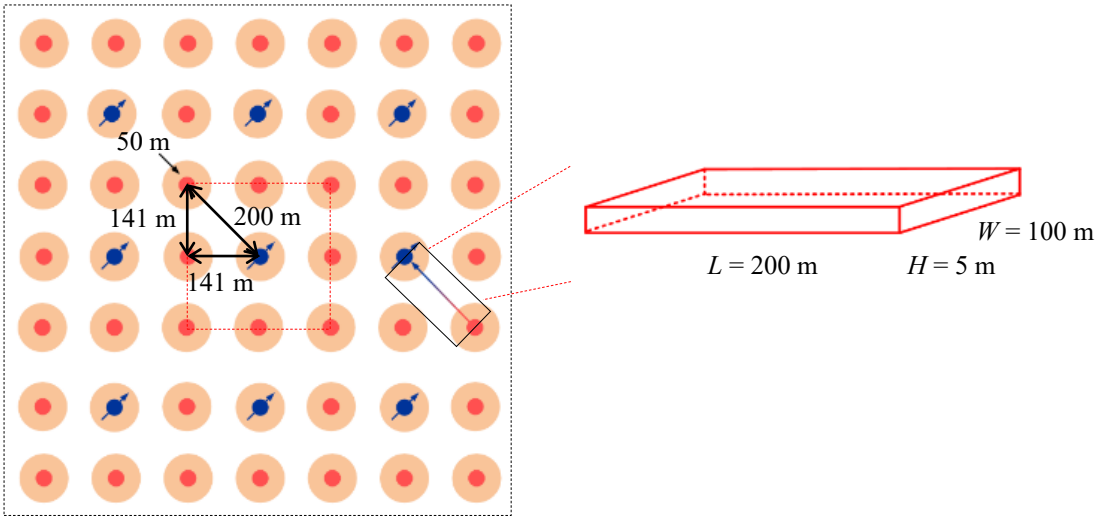

Fig. S6. Oil reservoir well parameters and extraction of unit zone. The red circle indicates the injection well, and the blue circle indicates the heavy oil production well.

Text S3: High-temperature and high-pressure metal fixture

A specialized high-temperature and high-pressure metal fixture was fabricated to withstand the rigorous conditions of steam huff-and-puff (e.g., 311 °C at 10 MPa). The fixture assembly primarily consists of a cover plate, a base plate, O-rings, silicone pad, and tightening bolts (Fig. S7). The base plate features a recessed cavity to house the chip, where the inlet and outlet ports are precisely aligned and sealed using O-rings. A silicone pad is placed atop the chip to distribute mechanical stress uniformly, preventing fracture during bolt tightening. The entire system is secured with high-strength bolts to maintain stability under extreme thermal and pressure loads.

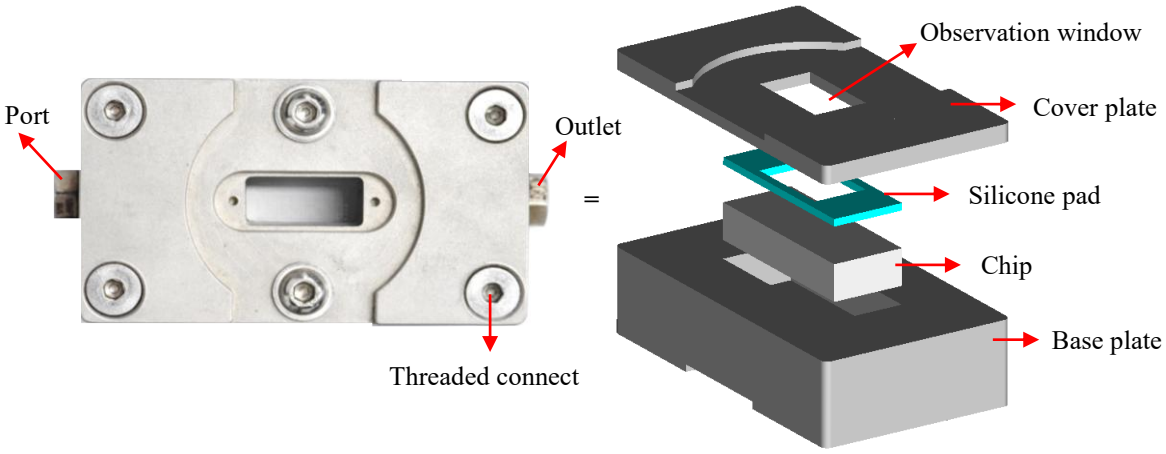

Fig. S7. Schematic illustration of the metal fixture structure and component assembly.

Text S4: Effect of reservoir temperature on heavy oil recovery

S4.1 Temperature distribution of microfluidic chip during steam injection

To assess the thermal response of the system, the heavy oil temperature was monitored during saturated steam injection at 6 MPa (Fig. S8). Results showed a negligible temperature increase, rising only from 26.7 to 27.3 °C. This ineffective heating is primarily attributed to the external aluminum holder, which acted as a significant heat sink due to its high thermal mass and conductivity.

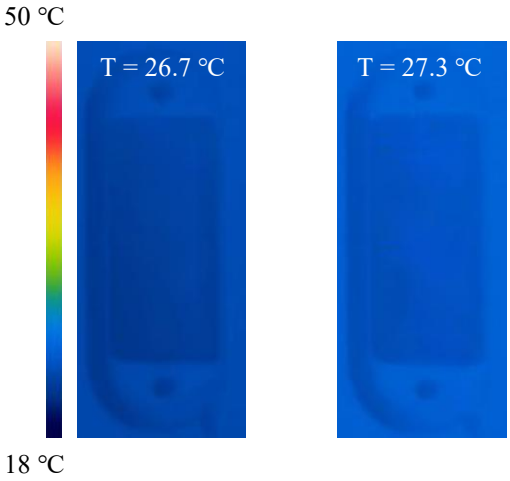

Fig. S8. The temperature distribution of heavy oil before and after steam injection with 6MPa.

S4.2 Deionized water injection under constant temperature chip conditions

Steam injection into the microfluidic chip was designed to elevate the heavy oil temperature, thereby reducing its viscosity and enhancing its mobility. However, due to the high thermal mass and conductivity of the metal holder used in this study, the steam prematurely condensed into liquid before entering the chip. To verify that the thermal effect of steam is indeed beneficial for heavy oil recovery, we conducted supplementary experiments by preheating the microfluidic chip to 50 °C and 70 °C. The spatial temperature distribution of the chip under these heating conditions is characterized in Fig. S9.

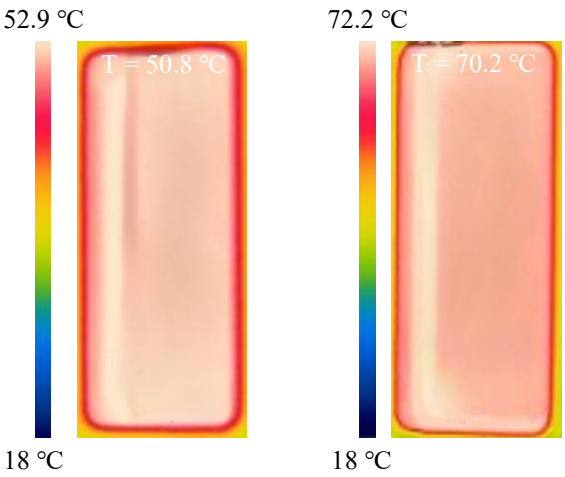

Fig. S9. Temperature distribution of pore network under constant temperature conditions.

Text S5: Phase distribution during huff-and-puff of heavy oil.

S5.1 Individual fluid during the injection stage

S5.1.1 Steam

To further illustrate the dynamic evolution of the heavy oil phase during steam injection, Fig. S10 presents the corresponding displacement process, where saturated steam at 6 MPa was injected into the microfluidic chip at a velocity of 5.5×10^{-3} m/s for a duration of 202 s. Upon entering the microfluidic chip, the steam underwent premature condensation into liquid water because of significant heat loss to the metal holder. As a result, the injected fluid failed to effectively heat the heavy oil. Consequently, the displacement pattern resembles water flooding at ambient temperature. After steam injection, the chip was sealed to simulate the reservoir soaking process, and the combined injection and soaking time was 30 min. The phase distribution at the end of injection defines the initial condition for the production stage.

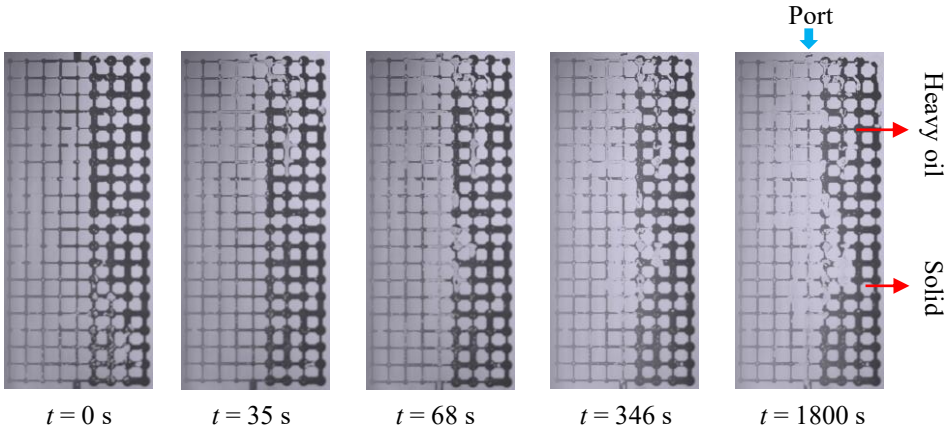

Fig. S10. Evolution of water and oil distribution during injection in the first huff-and-puff cycle. Unless otherwise specified, t = 0 s and 1800 s denote the initial and final stages, and the blue arrow indicates the port channel.

S5.1.2 N_2

To further illustrate the evolution of the heavy oil phase during N_2 injection, Fig. S11 shows the corresponding displacement process. N_2 was injected at a pressure of 1.84 MPa with a velocity of 7.78×10^{-2} m/s for a duration of 211 s. During the injection process, N_2 exhibited superior displacement performance. It not only mobilized heavy oil in high permeability regions but also extended the sweep into low permeability regions. Upon the end of the injection, gas bubbles were observed along the pore walls. The phase distribution after injection and the subsequent soaking period served as the initial state for the production phase.

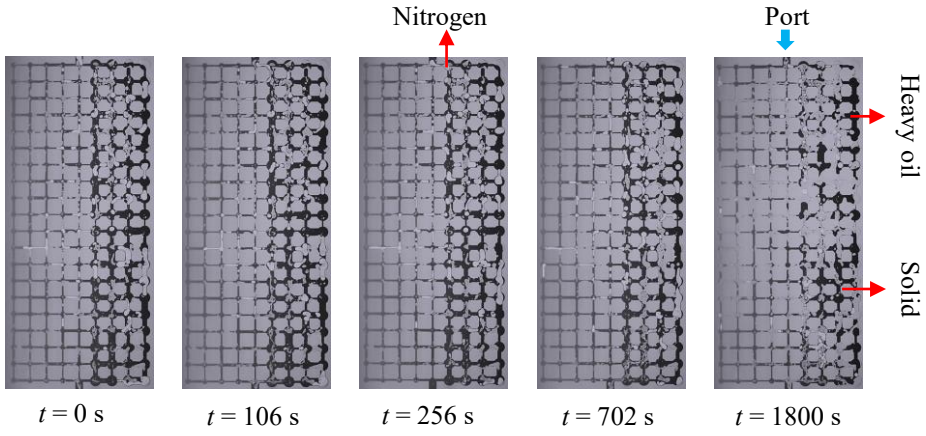

Fig. S11. Evolution of N_2 and oil distribution during injection in the first huff-and-puff cycle.

S5.1.3 ODA

To further illustrate the evolution of the heavy oil phase during ODA injection, the displacement process is presented in Fig. S12. ODA was injected at a pressure of 6.13 MPa with a velocity of 1.11×10^{-4} m/s for a duration of 180 s. During the injection process, ODA displacement mainly occurred in the high-permeability regions, while the heavy oil in the low-permeability zone showed no significant mobilization. The phase distribution after ODA injection and the subsequent soaking period served as the initial state for the subsequent extraction stage.

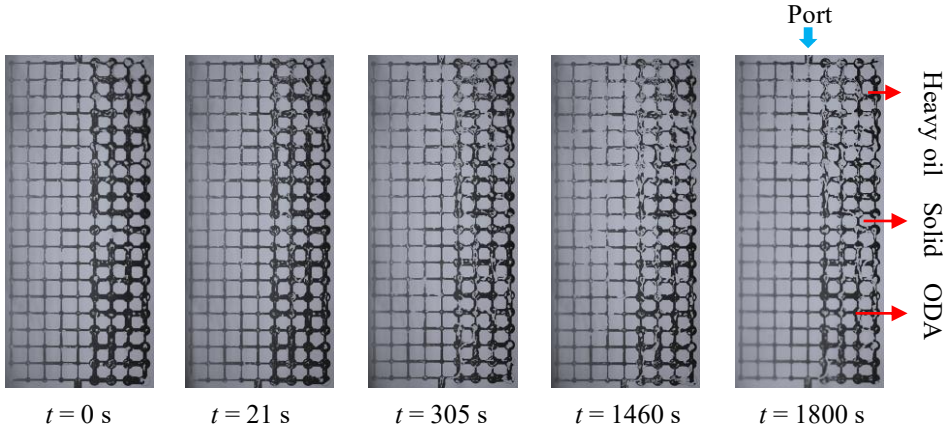

Fig. S12. Evolution of ODA and oil distribution during injection in the first huff-and-puff cycle.

S5.2 Dual fluids during the injection or extraction stage

S5.2.1 N_2-ODA during the injection stage

To further illustrate the evolution of the heavy oil phase during the dual-injection sequence (N_2-ODA), the displacement process is presented in Fig. S13. The injection parameters for both ODA and N_2 were maintained consistent with their respective single-phase baseline values. Nitrogen was injected into the microfluidic chip to displace the heavy oil, forming nitrogen channels in both the high and low permeability regions. Subsequently, ODA was injected and underwent pronounced in situ emulsification with the heavy oil, as indicated by the formation of a distinct brown oil phase. As the ODA advanced, it displaced the emulsified oil while simultaneously pushing the N_2, gradually removing the gas phase from the chip. Continued ODA injection further enhanced the sweep efficiency through persistent emulsification. The phase distribution after the dual-injection process and the subsequent soaking period served as the initial state for the subsequent production phase.

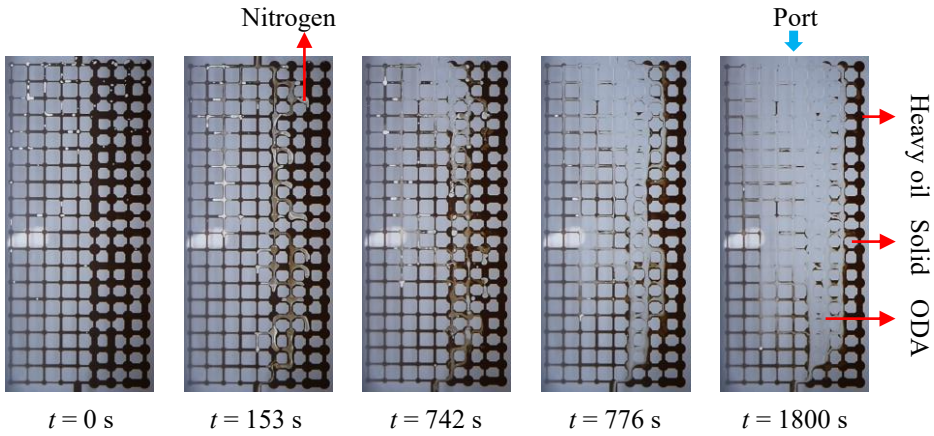

Fig. S13. Evolution of ODA, N_2, oil distribution during injection in the first huff-and-puff cycle.

S5.2.2 ODA-Steam during the extraction stage

For the ODA–steam huff-and-puff experiments, no oil production was observed at the outlet of pathway II, as shown in Fig. S14. This was attributed to dilution of the ODA by condensed water, which weakened its emulsification capacity. Consequently, a clear interface remained between the injected fluids and the heavy oil during the production process, and no highly mobile emulsified oil generated by in situ emulsification was observed.

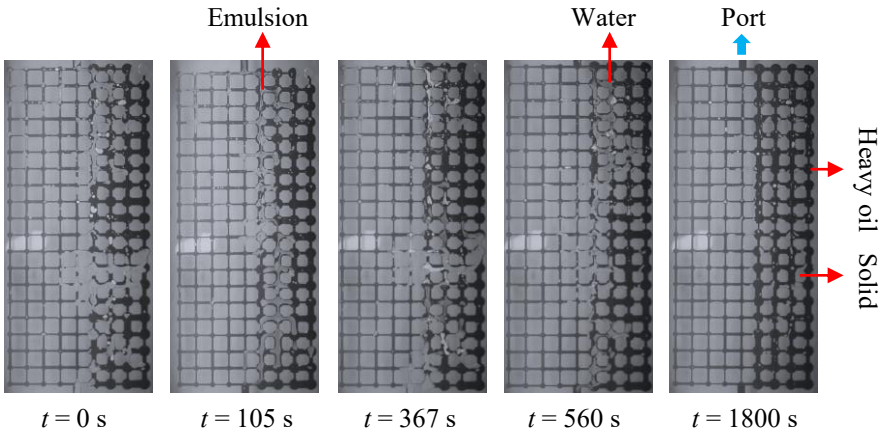

Fig. S14. Evolution of ODA, steam, oil distribution during injection in the first huff-and-puff cycle.

S5.2.3 N_2-Steam during the extraction stage

The N_2-steam case behaved similarly to the pure N_2 case, with no oil produced. However, notable differences were still observed between the two systems during heavy-oil production. As shown in Fig. S15, although N_2 expansion initially improved sweep efficiency in the low-permeability zones, the rapid formation of steam condensate introduced additional complexity. Liquid films infiltrated the N_2 bubbles, as indicated by the red circle in Fig. S15(a), and these water-laden bubbles subsequently collided and ruptured near the production port, forming dense microbubble clusters. This process promoted fragmentation of the heavy-oil phase, manifested as an oil-in-bubble phenomenon. Meanwhile, the rapid expansion intensified the instability of the N_2-oil interface. The resulting violent interfacial rearrangement occurred over a short timescale, suppressing further N_2 bubble growth and reducing the effective displacement energy. Consequently, the synergistic interaction between the two phases was disrupted, resulting in a markedly lower recovery efficiency than that observed in systems incorporating ODA.

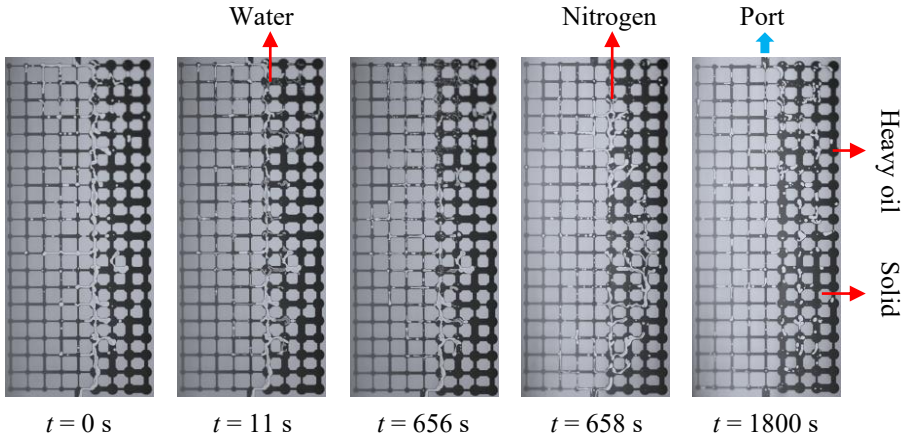

Fig. S15. Evolution of N_2, steam, oil distribution during injection in the first huff-and-puff cycle.

S5.3 Ternary injected fluids in extraction stage

S5.3.1 N_2-ODA-Steam

The N_2-ODA-steam extraction process generally resembled that of the N_2-ODA system. Except for the dilution of ODA induced by steam injection, which was reflected in the excessively large N_2 bubbles, the overall heavy-oil production behavior remained similar. In both cases, emulsified oil was produced first, followed by oil production driven by microbubbles and, finally, by N_2 expansion, as shown in Fig. S16.

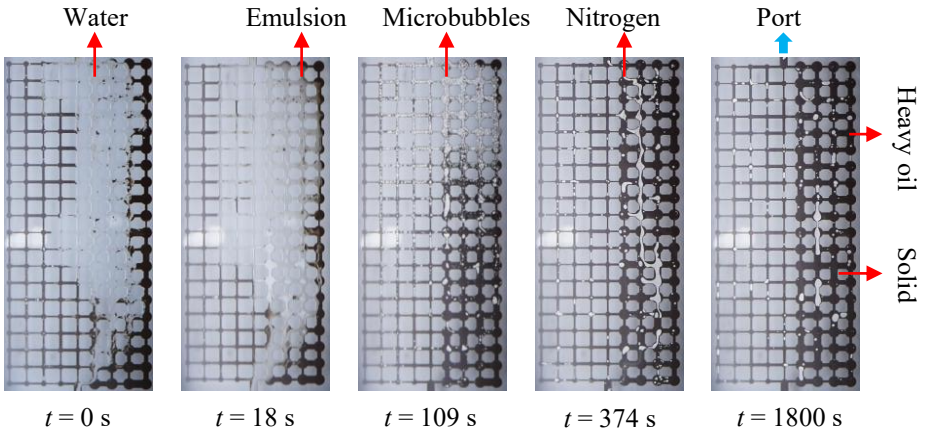

Fig. S16. Evolution of N_2, ODA, steam, oil distribution during injection in the first huff-and-puff cycle.

S5.3.2 N_2-steam-ODA

In the N_2-steam-ODA sequence, steam was injected into the microfluidic chip before ODA. This allowed water to first enter the pore network and dilute the subsequently injected ODA. As a result, the effective ODA concentration in the pores was lower than that in the N_2-ODA-steam case. Figure S17 confirms this observation: N_2-steam-ODA process exhibited low sweep efficiency (Fig. S17a) and did not produce emulsified oil. These results suggest that prior steam injection weakened the displacement performance of ODA.

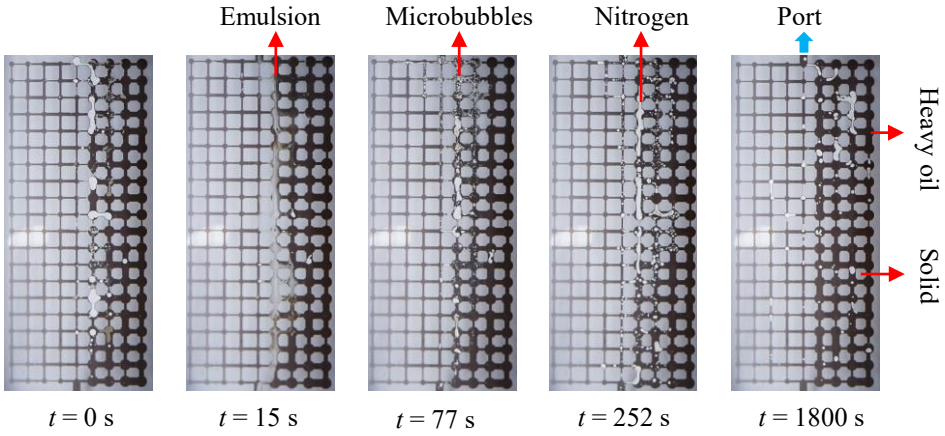

Fig. S17. Evolution of N_2, steam, ODA, oil distribution during injection in the first huff-and-puff cycle.